Geophysical Research Letters

RESEARCH LETTER
10.1029/2022GL101650

Recent Aqueous Activity on Mars Evidenced by Transverse Aeolian Ridges in the Zhurong Exploration Region of Utopia Planitia

Jiang Wang[1,2,3,4], Jiannan Zhao[2], Long Xiao[1,5], Shuai Peng[1], Liang Zhang[1], Zhixin Zhang[6], Antong Gao[1], He Qiao[1], Le Wang[1], Shiqi Zhang[2], Xiao Xiao[1], Yutong Shi[1], Siyuan Zhao[1], Jiawei Zhao[1], Yuqi Qian[1], Jun Zhang[1], Xubing Zhang[6], and Jun Huang[1,5]

[1]State Key Laboratory of Geological Processes and Mineral Resources, Planetary Science Institute, School of Earth Sciences, China University of Geosciences, Wuhan, China, [2]Key Laboratory of Geological Survey and Evaluation of Ministry of Education, China University of Geosciences, Wuhan, China, [3]State Key Laboratory of Lunar and Planetary Science, Macau University of Science and Technology, Macau, China, [4]Hubei Key Laboratory of Critical Zone Evolution, China University of Geosciences, Wuhan, China, [5]Chinese Academy of Sciences Center for Excellence in Comparative Planetology, Beijing, China, [6]School of Geography and Information Engineering, China University of Geosciences, Wuhan, China

Key Points:

- Morphology and evolution of the transverse aeolian ridges (TARs) in the Zhurong landing region are studied
- Polygonal features with hydrated minerals are identified on some of the TARs investigated by the Zhurong rover
- The polygons could be related to very recent aqueous activity and atmosphere-surface water exchange on Mars

Supporting Information:

Supporting Information may be found in the online version of this article.

Correspondence to:

J. Zhao,
jnzhao@cug.edu.cn

Citation:

Wang, J., Zhao, J., Xiao, L., Peng, S., Zhang, L., Zhang, Z., et al. (2023). Recent aqueous activity on Mars evidenced by transverse aeolian ridges in the Zhurong exploration region of Utopia Planitia. *Geophysical Research Letters*, *50*, e2022GL101650. https://doi.org/10.1029/2022GL101650

Received 12 OCT 2022
Accepted 13 MAR 2023

Author Contributions:

Conceptualization: Jiannan Zhao
Data curation: Shuai Peng, Liang Zhang, Zhixin Zhang, Antong Gao, He Qiao, Le Wang, Shiqi Zhang, Xiao Xiao, Siyuan Zhao, Yuqi Qian, Jun Zhang, Xubing Zhang
Formal analysis: Jiang Wang, Jiannan Zhao, Jun Huang
Funding acquisition: Jiang Wang, Jiannan Zhao, Long Xiao, Xubing Zhang, Jun Huang

Abstract Aqueous activities on Mars have gradually declined since the Noachian (>3.7 Ga). Although water can be stored in the subsurface during the latest epochs, geomorphological evidence is still limited. In this study, we used in situ imaging and spectral data acquired by China's Zhurong rover, as well as high-resolution remote-sensing data, to investigate the transverse aeolian ridges (TARs) in the Zhurong landing region of Utopia Planitia. A two-stage evolutionary scenario of the TARs is proposed and polygonal features with hydrated minerals are identified for the first time on the surface of Martian TARs. We discussed the possible formation mechanisms of the polygonal features, and proposed that they could be related to recent aqueous activity and atmosphere-surface water exchange on Mars, which sheds light on the hydrological cycle of Mars in current cold and dry climate.

Plain Language Summary The history of water on the surface of Mars has been studied for a long time. Since about 3.7 billion years ago, the role of water has gradually declined. Although the existence of subsurface ice on present-day Mars has been confirmed, evidence for surface water is still limited. Transverse aeolian ridges (TARs), a kind of ripple-like aeolian landform, are widely distributed on Mars and usually thought to be active within the last ~3 million years. They are also identified in southern Utopia Planitia, the landing region of China's Mars exploration rover Zhurong. We analyzed the morphology and evolution of the TARs in the Zhurong landing region, and found some polygonal features with hydrated minerals such as gypsum on the surface of the latest-formed TARs. We discussed the possible origins of these polygons, and proposed that they represent very recent aqueous activity on the Martian surface, which will help us better understand the hydrological cycle on current Mars.

1. Introduction

Mars is considered a desert planet at present due to its cold and dry climate that makes liquid water unstable on its surface (Carr & Head, 2010; Haberle et al., 2001). Nevertheless, water ice has been found in the polar caps (Bibring et al., 2004; Langevin et al., 2005) as well as the subsurface (Byrne et al., 2009; Dundas et al., 2014, 2018). In addition, several landforms may be related to recent water activity, for example, recurring slope lineae (RSL; McEwen et al., 2011; Ojha et al., 2015) and gullies (de Haas et al., 2015). However, the origin of RSLs and gullies is still under debate (e.g., Dundas et al., 2017, 2019), and geomorphological evidence for recent aqueous activity on Mars is insufficient.

Transverse aeolian ridges (TARs) are aeolian bedforms with small sizes, narrow transverse dimensions (Balme et al., 2008; Bretzfelder & Day, 2021; Chojnacki et al., 2015; Zimbelman & Foroutan, 2020), occurring throughout the low- to middle-latitude regions on the Martian surface (Berman et al., 2011; Wilson & Zimbelman, 2004). They are thought to be active within ~3 Ma (Berman et al., 2011; Reiss, 2004), and some are even active today (Chojnacki et al., 2021; Day, 2021; Silvestro et al., 2020). Most of them are usually decameter-scale and have relatively symmetric traverse profiles (Zimbelman, 2010; Zimbelman et al., 2012), which are quite different

Investigation: Jiang Wang, Jiannan Zhao, Long Xiao, Shuai Peng, Shiqi Zhang, Yutong Shi, Jun Zhang
Methodology: Jiang Wang, Shuai Peng, Liang Zhang, Zhixin Zhang, Antong Gao, He Qiao, Xubing Zhang
Resources: Jiannan Zhao, Long Xiao, Jun Huang
Software: Shuai Peng, Liang Zhang, Zhixin Zhang, Antong Gao, Le Wang, Xiao Xiao, Siyuan Zhao, Xubing Zhang
Supervision: Jiannan Zhao, Long Xiao
Validation: Jiang Wang, Antong Gao, He Qiao, Xiao Xiao, Jiawei Zhao
Visualization: Jiang Wang, Jiannan Zhao, Shuai Peng, Le Wang, Shiqi Zhang, Yutong Shi, Jiawei Zhao
Writing – original draft: Jiang Wang, Jiannan Zhao, Long Xiao, Liang Zhang, Jun Huang

from typical dunes or ripple forms (small ripple and large ripple, Lapotre et al., 2016) on Mars. Compared with the commonly seen dark-toned dunes, TARs commonly have relatively high albedos (Lu et al., 2021), representing a new class of aeolian bedform with unusual formation mechanism and special relationships between Martian atmosphere and sediment circulation (Balme et al., 2008; Berman et al., 2011; Geissler & Wilgus, 2017). TARs are also distributed in the southern Utopia Planitia (Figure 1) where China's first Mars exploration rover "Zhurong" landed (Gou et al., 2022; J. J. Liu et al., 2022; Zhao et al., 2021). During the first 100 sols (Martian days) of Zhurong's exploration, the rover moved about 1,000 m toward the south from the landing site at 109.925°E, 25.066°N (C. Li et al., 2022; J. J. Liu et al., 2022) and investigated the TARs along its traverse (Figure 1b) with equipped scientific payloads, which provides an unprecedented opportunity for exploring the morphological features of TARs. In this study, we mapped the TARs in a 2 × 2 km region (Figure 1a) that includes the traverse of the rover in its first 100 sols, and conducted detailed morphological analyses on the TARs visited by the rover. Fresh-appearing polygonal features on the TARs are reported, which provides significant new evidence for recent aqueous activity on Mars.

2. Data and Methods

We used the 0.25 m/pixel image from High Resolution Imaging Science Experiment (HiRISE, McEwen et al., 2007) to provide regional context and used the digital elevation model (DEM, data ID: DTEEC_069665_2055_069731_2055_A01; grid spacing: 1 m/pixel; vertical precision: ~0.2 m) generated from HiRISE stereo-pair images to conduct morphometric measurements of the TARs in the study region. A shaded-relief image of the HiRISE DEM (Figure S1 in Supporting Information S1) was created to inspect the topographic noise (Kirk et al., 2021). We also used newly acquired images by the Navigation and Terrain Cameras (NaTeCam) aboard the Zhurong rover to study detailed features of the TARs. The NaTeCam can obtain color images with 2,048 × 2,048 pixels and RGB channels that roughly cover wavelengths of 400–700 nm, and its imaging distance is 0.5 m–∞ (Liang et al., 2021).

Spectral data acquired by the Short-wave Infrared Spectrometer (SWIR), one of the important components of Mars Surface Composition Detector (MarSCoDe) aboard the Zhurong rover, were used to analyze the surface mineralogy of the TARs. The spectrometer covers wavelengths of 0.85–2.4 μm and has a spectral resolution of 3–12 nm with a field of view ~36.5 mrad (Xu et al., 2021). The original SWIR data obtained in this study are level 2B data products produced by Ground Research and Application System of China's Lunar and Planetary Exploration Program. Specifically, the dark current calibration and absolute radiometric calibration have been conducted. The accuracy of the absolute radiometric calibration is better than 5% (Y. Liu et al., 2022; Xu et al., 2021). In order to avoid the influence of interference noise in SWIR spectral data, we used the Savitzky-Golay algorithm (Savitzky & Golay, 1964) to smooth and denoise MarSCoDe SWIR spectra.

ArcGIS 10.6 software was used to measure TAR geometric parameters, including the TAR length (L) and width (W) (Figures 1d–1f). W is the longest distance perpendicularly toe-to-toe across the ridge crest. Length, perpendicular to the width, is the linear distance measured end-to-end of the ridge crest. The height (H) is the largest elevation difference along the width (Zimbelman, 2010; Zimbelman et al., 2012). Considering the inherent noise of HiRISE DEM, heights of some TARs were not calculated (Figure S1 in Supporting Information S1). The orientation of TAR is the azimuth of L. It should be noted that the lack of ground control and the existence of artifacts in HiRISE DTM may affect the accuracy of parameter measurements, especially for the height of small-sized landforms (Kirk et al., 2008). Therefore, these TAR parameters should be regarded as estimates.

3. Results

3.1. Distribution and Overall Morphology of the TARs

A total of 354 TARs (Data Set S1) were identified in the study region using the HiRISE image and they are mainly concentrated in the central and northwestern parts of the region (Figure 1c). Their lengths range from 4.7 to 81.7 m with an average of 27.9 m, and ~70% of them are 10–40 m in length (Table S1 and Figure S2a in Supporting Information S1). The TAR widths range from 1.8 to 25.2 m with an average of 6.7 m, and ~90% of the TARs are 2–11 m wide (Table S1 and Figure S2b in Supporting Information S1). Their heights, based on the HiRISE DEM (Figure 1c), can reach up to 4.4 m, although most of them (~85%) are concentrated between 0.3 and 1.4 m (Table S1 and Figure S2c in Supporting Information S1).

According to the morphology characteristics, the TARs in our study region can be classified into three types (Figures 1d–1f). Type 1 represents typical TAR with relatively straight ridge crest (Figure 1d). Type 2 is characterized

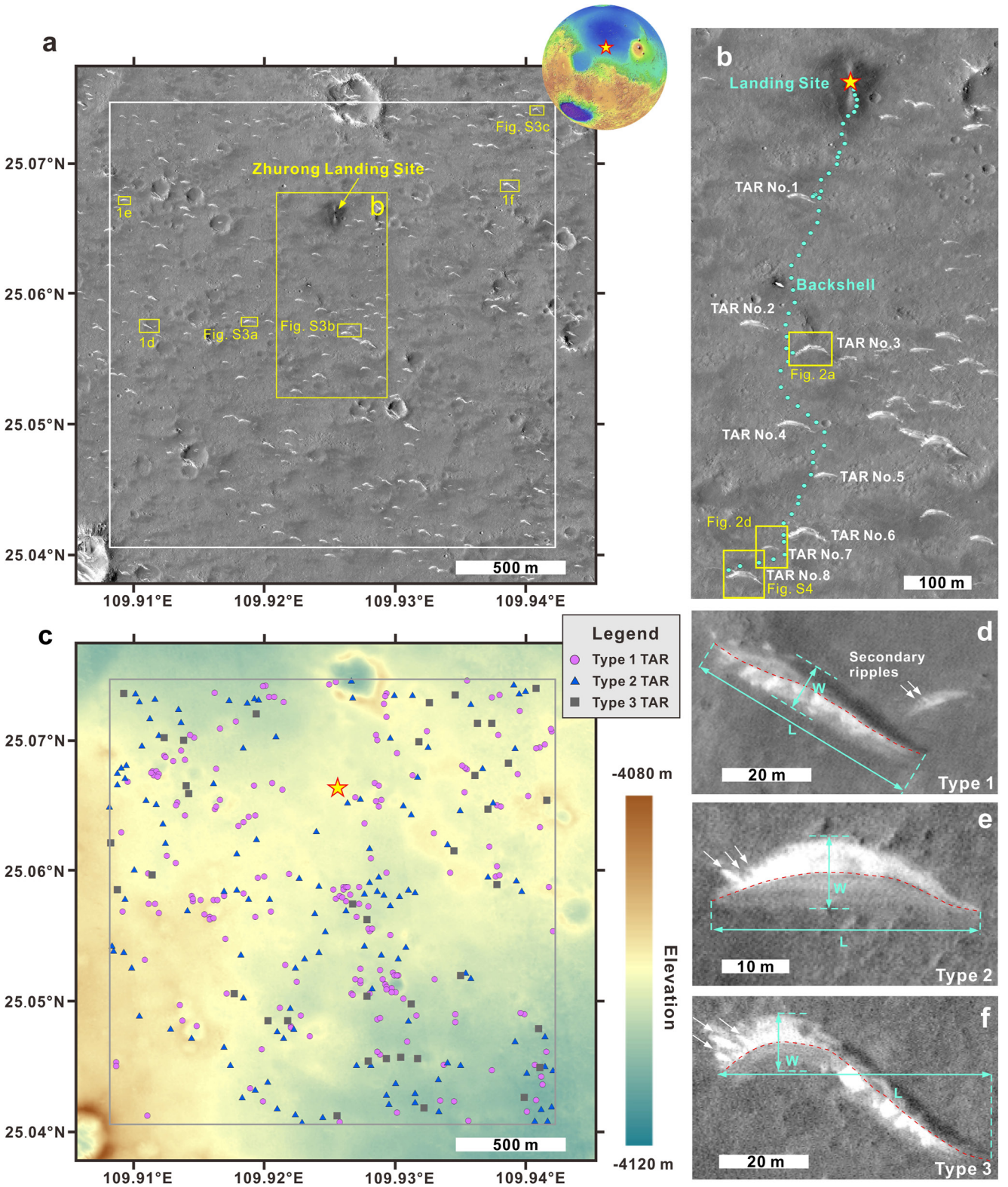

Figure 1.

by crescentic-shaped TARs with two horns generally bending to the south (Figure 1e). Type 3 TARs exhibit hook-like shapes with elongated eastern horns (Figure 1f). In addition, most of the TARs in our study region have their western horns modified by secondary sand ripples (Figure 1 and Figure S3 in Supporting Information S1).

3.2. Detailed TAR Morphology Investigated by the Zhurong Rover

During the first 100 sols of rover operations, Zhurong visited a total of eight TARs along its traverse (Figure 1b), and all of them belong to Type 2 TARs. They have widths of 25.1–63.8 and lengths of 5.0–10.9 m, and their heights can be up to 1.9 m. All of them developed secondary sand ripples in their western horns. For example, TAR No. 3 is generally E-W trending while multiple secondary ripples with an NW-SE trend and 1.2–10.6 m in width can be identified in the western part of the TAR (Figures 2a and 2b).

In situ observations by the NaTeCams aboard the rover found obvious tone variations on the TARs although they are generally brighter than the surroundings. Usually, the crest and the base of a TAR or its secondary ripples are dark-toned relative to the rest of the TAR while the TAR/ripple flanks are light-toned (Figure 2b). The close-up view of a secondary ripple on TAR No. 3 shows that the dark-toned area is concentrated with millimeter-scale coarse grains while the light-toned area is relatively smooth with indistinguishable grain sizes (should be smaller than 2 mm which is the size of the smallest well-resolved grains in the image, Figure 2c). Moreover, some striped patterns composed of dark-toned materials can be observed upon the light-toned area. The most notable features on the TAR are the polygonal features. They developed in light-toned areas and are usually five- or six-sided and ~5–10 cm in size (Figure 2c). Their marginal cracks are relatively straight and well connected, with their junction angles ranging from ~80° to 150°. By checking other NaTeCam images, we found that polygonal cracks are also identified on the surface of TAR No. 7 (Figure 2d–2f and Figure S4 in Supporting Information S1) and No. 8 (Figure S5 in Supporting Information S1). On TAR No. 7, polygonal features are up to 15 cm in size and they look more irregular than those on TAR No. 3. On TAR No. 8, the polygons are more irregular, but it is hard to estimate their sizes due to the low resolution caused by relatively larger distance between the rover and the TAR.

3.3. Mineral Composition of the Polygonal Surface on the TARs

We analyzed the spectral data acquired in the polygonal surface of TARs No. 3 (Figure 2c) and No. 7 (Figure 2f) by the SWIR to detect potential hydrated minerals. As shown in Figure 3a, the SWIR spectra of TARs Nos. 3 and 7 show obvious H_2O absorptions around 1.94 μm, weak OH absorptions around 1.45 μm and obvious OH absorptions around 2.20 μm. Among them, the 2.20 μm absorptions represent the diagnostic characteristics of hydroxyl stretching commonly found in spectra of hydrated sulfates or Al-phyllosilicates (Viviano-Beck et al., 2014). To further determine the possible mineral type, we selected several laboratory spectra of hydrated sulfates and Al-phyllosilicates that are most similar to the acquired SWIR spectra, including montmorillonite, illite, vermiculite, ferricopiapite, gypsum, and mixtures of gypsum (20 and 50 vol.%) and Mars Global Simulant (Figure 3b). Typically, in the range of 1.0–2.4 μm, Al-phyllosilicates (montmorillonite, illite, and vermiculite) have absorptions around 1.4, 1.9, and 2.2 μm (Viviano-Beck et al., 2014), ferricopiapite has obvious absorption around 1.45, 1.75, and 1.94 μm, while gypsum has absorptions around 1.45, 1.75, 1.94, 2.2, and 2.4 μm (Gendrin et al., 2005; Langevin et al., 2005). Therefore, as shown in Figure 3, the 1.45 and 1.94 μm absorptions of the SWIR spectra are more consistent with sulfates rather than Al-phyllosilicates, and the obvious 2.2 μm absorption excludes the ferricopiapite. Moreover, the spectra of gypsum and gypsum mixtures show obvious shifts around 1.94 μm and the laboratory spectrum of 50 vol.% gypsum mixture best fits the SWIR spectra, indicating a sulfate-bearing composition of the polygonal surface.

4. Discussion

TARs are oriented perpendicular to the prevailing wind direction when they are formed (Balme et al., 2008), which makes it possible to retrieve information about the paleo wind regime (Berman et al., 2011). The orientation rose diagram of TARs shows two predominant directions (E-W and NW-SE, Figure S6a in Supporting

Figure 1. Distribution and classification of the transverse aeolian ridges (TARs) in the study region. The yellow stars in the figures denote the location of the Zhurong landing site and yellow boxes denote the location of other figures. North is up in all images. The background is High Resolution Imaging Science Experiment (HiRISE) image (ID: ESP_069665_2055_RED). (a) HiRISE image of the study region (white box) with the inset of colourized MOLA topographic map showing the location of the landing site; (b) Landing site of the Zhurong rover and the traverse in its first 100 sols. The cyan dots denote the navigation points of the rover. TARs investigated by Zhurong are labeled. (c) Classification and location of the TARs in the study region. The background is colourized HiRISE digital elevation model (ID: DTEEC_069665_2055_069731_2055_A01); (d–f) Typical Type 1 to Type 3 TARs showing the measurements of TAR length (L) and width (W) in this study. The red dashed lines mark the ridge crest, and the white arrows indicate the secondary ripples.

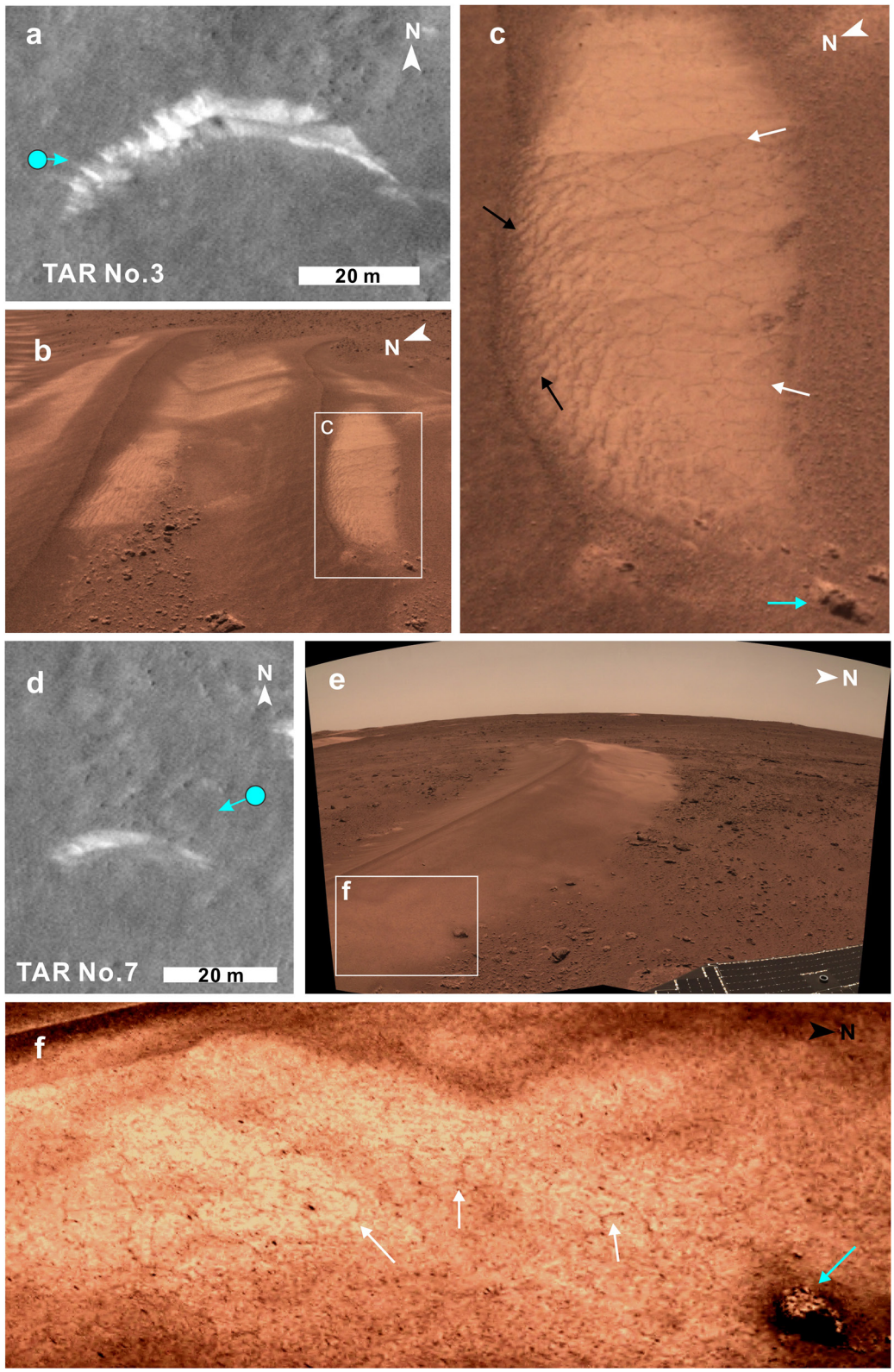

Figure 2.

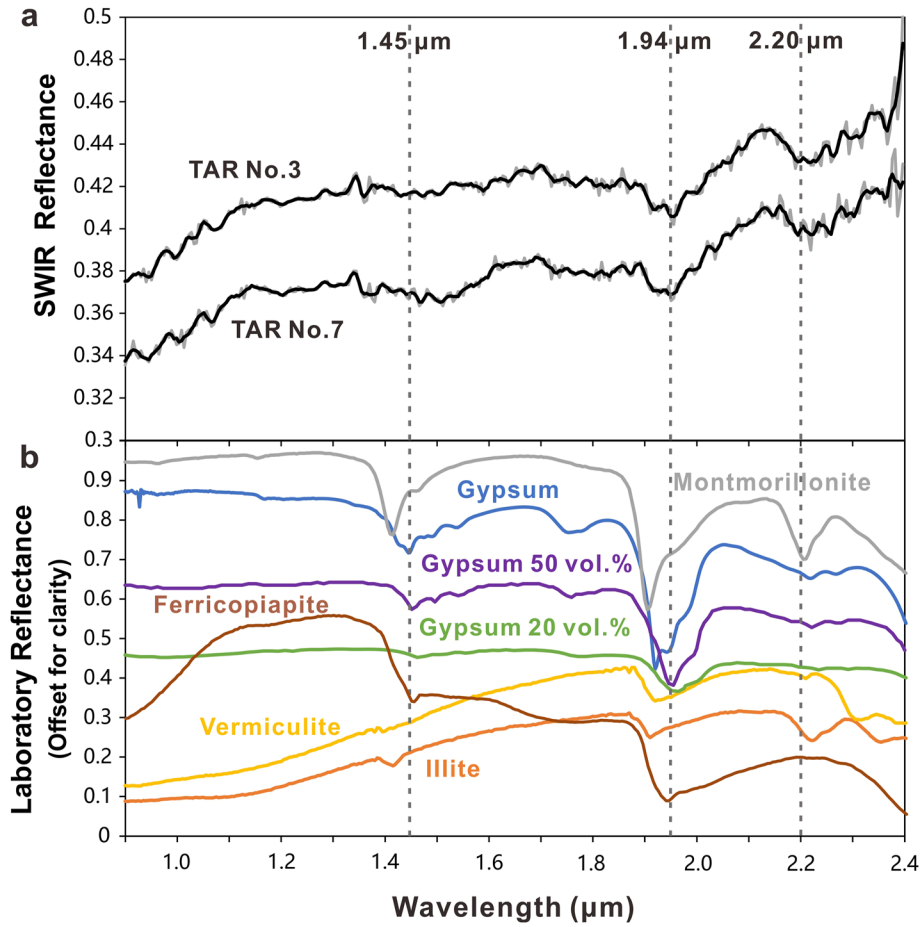

Figure 3. Short-wave Infrared Spectrometer (SWIR) spectra of the polygonal surfaces on transverse aeolian ridges (TARs) No. 3 and No. 7 (a), and comparison with laboratory spectra of phyllosilicates (montmorillonite, illite, and vermiculite) and sulfates (ferricopiapite, gypsum, mixtures of gypsum (20 and 50 vol.%) and Mars Global Simulant (J. J. Liu et al., 2022; Y. Liu et al., 2022; Wu et al., 2021)) (b). Gray solid lines in the top panel represent raw data and black solid lines represent smoothed SWIR spectra. Sources for the laboratory spectra used in this study are listed in Table S2 in Supporting Information S1. SWIR spectral data ID: TAR No.3: HX1-Ro_GRAS_MarSCoDe-SWIR321-06_SCI _N_20210719164905_20210719164905_00065_A.2B and TAR No.7: HX1-Ro_GRAS_ MarSCoDe-SWIR321-06_SCI_N_0210816094511_20210816094511_00092_A.2B.

Information S1), indicating the change of local prevailing winds. Type 3 TARs were not included, because they probably have experienced complex modifications by winds and it is difficult to quantify their orientations. Further observations found that the dominant ridge trends of Type 1 are E-W and NW-SE (Figure S6b in Supporting Information S1), and those of Type 2 are roughly E-W (Figure S6c in Supporting Information S1). We have also noted that Type 1 TARs tend to have smaller sizes than Type 2 and Type 3 (Figure S2 in Supporting Information S1), although some of the E-W and NW-SE oriented Type 1 TARs can be as large as most Type 2 and Type 3 TARs (Figures 1d–1f).

Figure 2. Detailed morphology of transverse aeolian ridge (TAR) No. 3 and No. 7 along the Zhurong traverse. (a, d) High Resolution Imaging Science Experiment (HiRISE) image of TAR No. 3 and No. 7. HiRISE ID: ESP_069665_2055_RED. The cyan dots and arrows denote the location and viewing direction of the rover when obtaining the NaTeCam images of the TARs; (b) A portion of the TAR No. 3 with the white box denotes the location of (c). NaTeCam ID: HX1-Ro_GRAS_NaTeCamB-F-006_SCI_N_ 20210719130730_20210719130730_00065_A.2C; (c) Zoomed-in NaTeCam image showing polygonal features (white arrows) on the surface of TAR No. 3. The black arrows point to striped patterns composed of coarse grains. The cobble for scale (cyan arrow) has a long axis of ~8 cm; (e) A NaTeCam panorama showing the location of (f) (white box). NaTeCam IDs: HX1-Ro_GRAS_NaTeCamB-F-03_SCI_N_ 20210816102520_20210816102520_00092_A.2C and HX1-Ro_GRAS_ NaTeCamB-F-004_SCI_N_20210816102655_20210816102655_00092 _A.2C; (f) Zoomed-in NaTeCam image showing the polygonal features (black arrows) on the surface of TAR No. 7. The image is stretched to increase the contrast to better show the polygonal features and the original image is shown in Figure S4 in Supporting Information S1. The cobble for scale (cyan arrow) is about 13 cm in size. NaTeCam ID: HX1-Ro_GRAS_NaTeCamA-F-005_SCI_N_20210816102813_20210816102813_00092_A.2C.

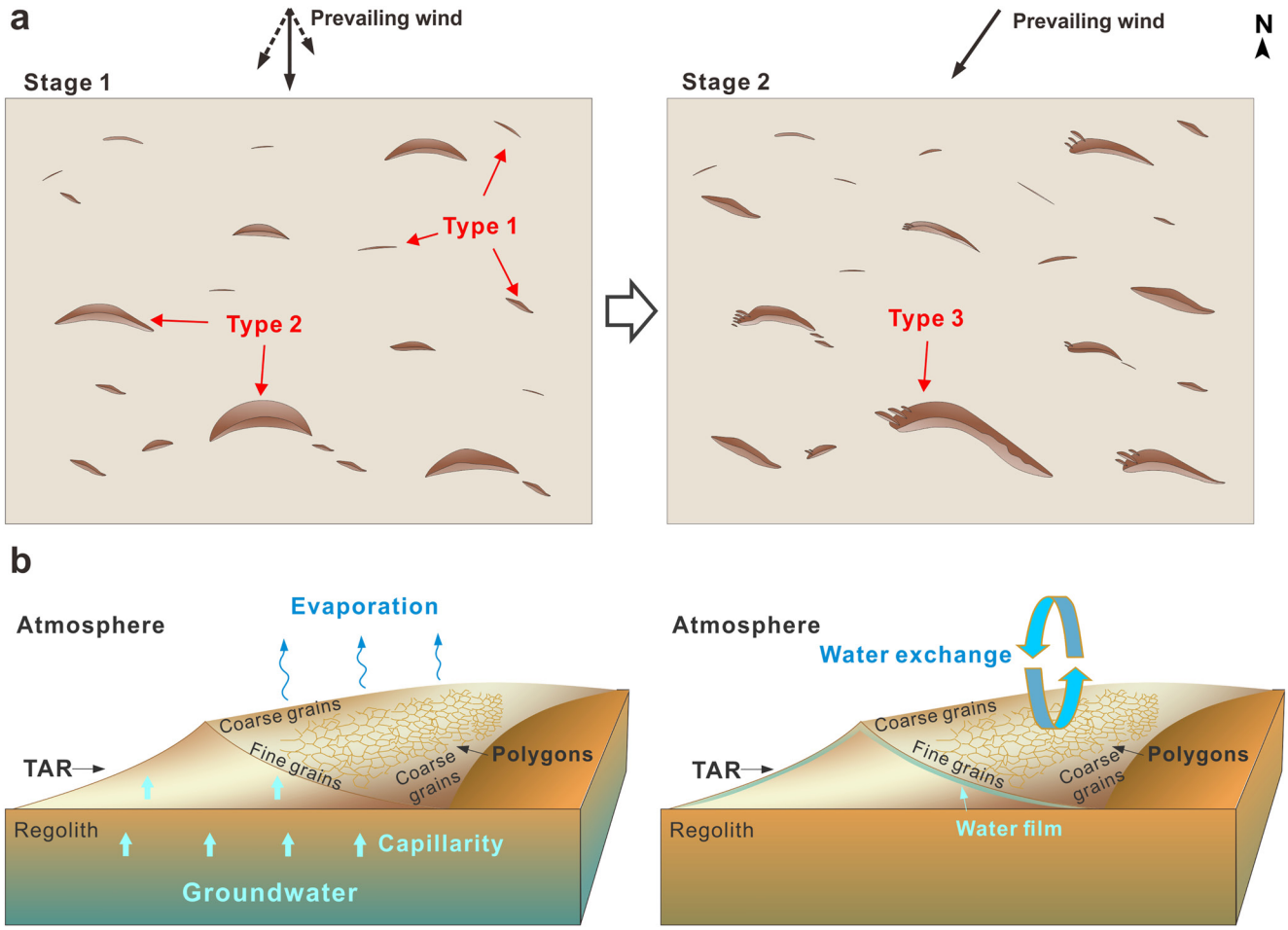

Figure 4. Schematic model showing the two-stage evolution scenario for the transverse aeolian ridges (TARs) and the possible formation mechanisms of polygonal features on TAR surfaces. (a) Evolution of the TARs. Stage 1: north wind played the dominant role, forming nearly E-W oriented TARs. Stage 2: prevailing wind direction changed to northeast, forming NW-SE trending TARs. The solid black arrows indicates the dominant wind, and the dashed arrows represent the variation of wind. (b) The left model shows that groundwater was transported to the TAR by capillary action and then evaporated to the atmosphere. During this process, polygonal features formed on the TAR surface with fine grains. The right model shows an alternative formation mechanism: when a water/brine film exists, the upper layer of a TAR is cemented to form an indurated sand crust that then fractures into polygons due to temperature/moisture changes or deliquescence/dehydration cycling of salts. Atmosphere-surface water exchange plays an important role during this process.

Based on the remote-sensing and in situ investigations, a two-stage scenario for the evolution of the TARs in our study region is proposed (Figure 4a). During Stage 1, the local prevailing wind direction was generally from the north with small-scale variations, forming nearly E-W oriented TARs with different sizes. In this stage, some NW-SE and NE-SW oriented TARs also formed due to small-scale wind variations and/or topographic influence. Among these TARs, early formed larger-sized E-W oriented TARs became crescentic-shaped (Type 2) as their horns moved faster than the central parts (Hersen, 2004), while the later formed small-sized TARs with relatively straight crestlines were still in their primary forms (Type 1). In Stage 2, the prevailing wind direction changed to NE (Figure 4a). The NW-SE oriented Type 1 TARs formed in Stage 1 continuously grew up in size while the horns of Type 2 TARs were modified in this stage. As the western part of a Type 2 TAR was nearly parallel to the NE-SW wind direction, it will be modified to form NW-SE oriented secondary sand ripples which can then partly cover the original western horn (Figure 1 and Figure S3a in Supporting Information S1). Meanwhile, as the eastern horn is perpendicular to the wind direction, it will grow and extend in the SE direction, forming Type 3 TARs. Another possible formation mechanism of the Type 3 TARs is that some preexisting or newly formed NW-SE oriented TARs adjacent to the eastern horns of Type 2 TARs may grow and finally connect with each other, forming the extended eastern horn of Type 3 as suggested by Figures S3b and S3c in Supporting Information S1. It should be noted that the orientations of small sized TARs could just be random as they are easily affected by local topographic relief.

The most intriguing features of the TARs are the polygons. Polygonal features on Mars can develop in various scales and geological settings. For example, polygons of 5–15 m in diameter have been observed in Athabasca Valles and are considered to be formed by contraction during lava cooling (Ryan & Christensen, 2012); possible ice-wedge polygons formed by freeze-thaw cycling are widely distributed in middle latitudes of Utopia Planitia and Argyre Basin (Soare et al., 2014, 2021); thermal contraction of ice-rich permafrost also formed meter-sized polygons across Martian middle to high latitudes (Haltigin et al., 2014; Levy et al., 2009); polygonal features ranging from several meters to hundreds of meters in size with a desiccation origin have been identified in local lows with chloride or clay-rich deposits (Dang et al., 2020; El Maarry et al., 2010; Ye et al., 2019); large-scale (several to tens of kilometers in size) polygonal terrains are widely distributed in the Utopia Planitia and could be related to volumetric compaction of sedimentary deposits in the Utopia Basin (Buczkowski et al., 2012). In addition, in situ investigations by the Opportunity rover identified centimeter- to decimeter-scale polygons in sedimentary layers and they are considered as contractional cracks (Grotzinger et al., 2006; McLennan et al., 2005). Nevertheless, polygonal features on the surface of Martian aeolian bedforms have not been reported.

In the Zhurong landing site, polygonal cracks on the surface of TARs are centimeter- to decimeter-sized, five- to six-sided, and are only observed in the areas with fine-grained materials. Considering their relatively small size and the aeolian-bedform-related geological setting, we can eliminate the origin of lava cooling polygons, permafrost polygons, and volumetric compaction of sedimentary deposits. One possible mechanism that could lead to the formation of the polygons is contraction during water evaporation (Figure 4b), which is supported by similar polygonal features identified on the surface of sulfate-bearing sand dunes of White Sands National Monument, New Mexico (Chavdarian & Sumner, 2006, 2011). Chavdarian and Sumner proposed that they formed when water is lost to the atmosphere, and are better developed with fine-grained sulfate-rich dunes that are cohesive enough to crack due to capillary forces (Chavdarian & Sumner, 2011). However, a problem related to this mechanism is that bulk liquid water is required for the formation of polygons. As the polygons can develop on the secondary ripples of the TARs (Figure 2c) that could be younger than 1 Ma (Berman et al., 2011; Gou et al., 2022; Lu et al., 2022) or even still active today (Day, 2021), they should be very young features formed after the last stage of TAR evolution in the latest Martian geologic epoch. During this period, rainfall precipitation is not likely to happen due to low atmospheric pressure and temperature (Craddock & Lorenz, 2017; Palumbo et al., 2020), and groundwater could be the only source supplying water for the formation of the polygons (the left part of Figure 4b). However, as the mean temperature of the last 2.5 Ma at the Zhurong site is only 214.4 K (Mellon & Sizemore, 2022), groundwater may not stably exist. Although ice can accumulate in the subsurface (X. Li et al., 2023; Mellon & Sizemore, 2022), it may not melt significantly in bulk as high percent perchlorate or ferric sulfates which were not identified in our spectral analyses are needed to lower the freezing point (Möhlmann & Thomsen, 2011). Moreover, this scenario is difficult to explain the mechanism for the concentration of capillary groundwater on the aeolian bedforms which stand above the surrounding surface.

An alternative formation mechanism of the polygons could be the fracture of indurated crusts. Indurated soil crusts on Mars have been observed in almost all the landing regions of Mars landers and rovers, for example, Viking landing sites (Mutch et al., 1976), Meridiani Planum (Herkenhoff et al., 2004), Gusev crater (Cabrol et al., 2006), and Gale crater (Blake et al., 2013). These crusts could result from the existence of water film at microscopic scale in soil tubules (Figure 4b, Cabrol et al., 2006). Especially when salts dissolve in water and then precipitate on soil particles, the upper soil surface will be weakly cemented (Herkenhoff et al., 2004), forming an indurated crust that may then fracture into polygons due to temperature/moisture changes or deliquescence/dehydration cycling of salts (Chan et al., 2008). During this process, exchange of water between Martian atmosphere and the surface plays an important role and only little amount of water is needed (Cabrol et al., 2006). Indurated crusts were also proposed to occur on sand dunes based on computer simulation (Schatz et al., 2006), and were indicated by in situ observations of the Curiosity rover which discovered fractures on Bagnold Dunes (Ewing et al., 2017). Although most of the reported fractures formed within the indurated soil/sand crusts are linear or irregular in shape, this mechanism could still be the most plausible mechanism for the formation of five- to six-sided polygons on the TARs of Zhurong landing site.

5. Summary and Concluding Remarks

We investigated the morphology, composition, and evolution of the TARs in the Zhurong landing region of Utopia Planitia, emphasizing on the polygonal features on TAR surface. Two main possible formation mechanisms of

the polygons were discussed: (a) contractional cracks formed during groundwater evaporation and (b) fracture of indurated sand crust, both of which are related to recent aqueous activity on Mars. We proposed that the latter is the most plausible origin of the polygons and it provides clues for better understanding the hydrological cycle of Mars and the water exchange between martian surface and atmosphere in the "cold and dry" Amazonian epoch.

Data Availability Statement

The HiRISE image and related topographic data used in this work can be obtained freely from Lunar and Planetary Laboratory of University of Arizona at the following links: https://www.uahirise.org/ESP_069665_2055; https://www.uahirise.org/ESP_075559_2055; and https://www.uahirise.org/dtm/dtm.php?ID=ESP_069665_2055. Imaging (NaTeCam) and spectral (SWIR) data of the Zhurong rover used in this work, and the basic parameters of the TARs in the study region listed in Data Set S1 can be accessed at: https://doi.org/10.5281/zenodo.7733921.

Acknowledgments
The authors gratefully acknowledge the China National Space Administration (CNSA) for organizing and implementing the Tianwen-1 mission. This research is funded by the National Key Research and Development Program of China (2022YFF0504000), the National Natural Science Foundation of China (42272274, 42202262, 42241111, and 42273041), the Pre-research Project on Civil Aerospace Technologies (D020101), China Postdoctoral Science Foundation (2021M702999), the Natural Science Foundation of Hubei Province (2022CFB687), the Open Project from State Key Laboratory of Lunar and Planetary Science, Macau University of Science and Technology (SKL-LPS(MUST)-2021-2023), and Wuhan Science and Technology Plan Project-Application Basic Frontier Project (2019010701011403). We are grateful to the editor Dr. Dombard and the anonymous reviewer for their comments and suggestions that greatly improved our manuscript.

References

Balme, M., Berman, D. C., Bourke, M. C., & Zimbelman, J. R. (2008). Transverse aeolian ridges (TARs) on Mars. *Geomorphology*, *101*(4), 703–720. https://doi.org/10.1016/j.geomorph.2008.03.011

Berman, D. C., Balme, M. R., Rafkin, S. C. R., & Zimbelman, J. R. (2011). Transverse aeolian ridges (TARs) on Mars II: Distributions, orientations, and ages. *Icarus*, *213*(1), 116–130. https://doi.org/10.1016/j.icarus.2011.02.014

Bibring, J.-P., Langevin, Y., Poulet, F., Gendrin, A., Gondet, B., Berthé, M., et al. (2004). Perennial water ice identified in the south polar cap of Mars. *Nature*, *428*(6983), 627–630. https://doi.org/10.1038/nature02461

Blake, D. F., Morris, R. V., Kocurek, G., Morrison, S. M., Downs, R. T., Bish, D., et al. (2013). Curiosity at Gale crater, Mars: Characterization and analysis of the Rocknest sand shadow. *Science*, *341*(6153), 1239505. https://doi.org/10.1126/science.1239505

Bretzfelder, J. M., & Day, M. (2021). Alien aeolian bedforms: A comparative sedimentary analysis of the dingo gap bedform and hidden valley ripple traverses, Gale Crater, Mars. *Journal of Geophysical Research: Planets*, *126*(8), e2021JE006904. https://doi.org/10.1029/2021je006904

Buczkowski, D. L., Seelos, K. D., & Cooke, M. L. (2012). Giant polygons and circular graben in western Utopia basin, Mars: Exploring possible formation mechanisms. *Journal of Geophysical Research*, *117*(E8), E08010. https://doi.org/10.1029/2011je003934

Byrne, S., Dundas, C. M., Kennedy, M. R., Mellon, M. T., McEwen, A. S., Cull, S. C., et al. (2009). Distribution of mid-latitude ground ice on Mars from new impact craters. *Science*, *325*(5948), 1674–1676. https://doi.org/10.1126/science.1175307

Cabrol, N. A., Farmer, J. D., Grin, E. A., Richter, L., Soderblom, L., Li, R., et al. (2006). Aqueous processes at Gusev crater inferred from physical properties of rocks and soils along the Spirit traverse. *Journal of Geophysical Research*, *111*(E2), E02S20. https://doi.org/10.1029/2005je002490

Carr, M. H., & Head, J. W. (2010). Geologic history of Mars. *Earth and Planetary Science Letters*, *294*(3–4), 185–203. https://doi.org/10.1016/j.epsl.2009.06.042

Chan, M. A., Yonkee, W. A., Netoff, D. I., Seiler, W. M., & Ford, R. L. (2008). Polygonal cracks in bedrock on Earth and Mars: Implications for weathering. *Icarus*, *194*(1), 65–71. https://doi.org/10.1016/j.icarus.2007.09.026

Chavdarian, G. V., & Sumner, D. Y. (2006). Cracks and fins in sulfate sand: Evidence for recent mineral-atmospheric water cycling in Meridiani Planum outcrops? *Geology*, *34*(4), 229–232. https://doi.org/10.1130/g22101.1

Chavdarian, G. V., & Sumner, D. Y. (2011). Origin and evolution of polygonal cracks in hydrous sulphate sands, White Sands National Monument, New Mexico. *Sedimentology*, *58*(2), 407–423. https://doi.org/10.1111/j.1365-3091.2010.01169.x

Chojnacki, M., Hargitai, H., & Kereszturi, Á. (2015). Encyclopedia of planetary landforms, (pp. 1–6).

Chojnacki, M., Vaz, D. A., Silvestro, S., & Silva, D. C. (2021). Widespread megaripple activity across the north polar ergs of Mars. *Journal of Geophysical Research: Planets*, *126*(12), e2021JE006970. https://doi.org/10.1029/2021je006970

Craddock, R. A., & Lorenz, R. D. (2017). The changing nature of rainfall during the early history of Mars. *Icarus*, *293*, 172–179. https://doi.org/10.1016/j.icarus.2017.04.013

Dang, Y., Zhang, F., Zhao, J., Wang, J., Xu, Y., Huang, T., & Xiao, L. (2020). Diverse polygonal patterned grounds in the northern Eridania basin, Mars: Possible origins and implications. *Journal of Geophysical Research: Planets*, *125*(12), e2020JE006647. https://doi.org/10.1029/2020je006647

Day, M. (2021). Interaction bounding surfaces exposed in migrating transverse aeolian ridges on Mars. *Geology*, *49*(12), 1527–1530. https://doi.org/10.1130/g49373.1

de Haas, T., Ventra, D., Hauber, E., Conway, S. J., & Kleinhans, M. G. (2015). Sedimentological analyses of Martian gullies: The subsurface as the key to the surface. *Icarus*, *258*, 92–108. https://doi.org/10.1016/j.icarus.2015.06.017

Dundas, C. M., Bramson, A. M., Ojha, L., Wray, J. J., Mellon, M. T., Byrne, S., et al. (2018). Exposed subsurface ice sheets in the Martian mid-latitudes. *Science*, *359*(6372), 199–201. https://doi.org/10.1126/science.aao1619

Dundas, C. M., Byrne, S., McEwen, A. S., Mellon, M. T., Kennedy, M. R., Daubar, I. J., & Saper, L. (2014). HiRISE observations of new impact craters exposing Martian ground ice. *Journal of Geophysical Research: Planets*, *119*(1), 109–127. https://doi.org/10.1002/2013je004482

Dundas, C. M., McEwen, A. S., Chojnacki, M., Milazzo, M. P., Byrne, S., McElwaine, J. N., & Urso, A. (2017). Granular flows at recurring slope lineae on Mars indicate a limited role for liquid water. *Nature Geoscience*, *10*(12), 903–907. https://doi.org/10.1038/s41561-017-0012-5

Dundas, C. M., McEwen, A. S., Diniega, S., Hansen, C. J., Byrne, S., & McElwaine, J. N. (2019). The formation of gullies on Mars today. *Geological Society, London, Special Publications*, *467*(1), 67–94. https://doi.org/10.1144/sp467.5

El Maarry, M. R., Markiewicz, W. J., Mellon, M. T., Goetz, W., Dohm, J. M., & Pack, A. (2010). Crater floor polygons: Desiccation patterns of ancient lakes on Mars? *Journal of Geophysical Research*, *115*(E10), E10006. https://doi.org/10.1029/2010je003609

Ewing, R. C., Lapotre, M. G. A., Lewis, K. W., Day, M., Stein, N., Rubin, D. M., et al. (2017). Sedimentary processes of the Bagnold Dunes: Implications for the eolian rock record of Mars. *Journal of Geophysical Research: Planets*, *122*(12), 2544–2573. https://doi.org/10.1002/2017je005324

Geissler, P. E., & Wilgus, J. T. (2017). The morphology of transverse aeolian ridges on Mars. *Aeolian Research*, *26*, 63–71. https://doi.org/10.1016/j.aeolia.2016.08.008

Gendrin, A., Mangold, N., Bibring, J.-P., Langevin, Y., Gondet, B., Poulet, F., et al. (2005). Sulfates in Martian layered terrains: The OMEGA/Mars express view. *Science*, *307*(5715), 1587–1591. https://doi.org/10.1126/science.1109087

Gou, S., Yue, Z., Di, K., Zhao, C., Bugiolacchi, R., Xiao, J., et al. (2022). Transverse aeolian ridges in the landing area of the Tianwen-1 Zhurong rover on Utopia Planitia, Mars. *Earth and Planetary Science Letters*, *595*, 117764. https://doi.org/10.1016/j.epsl.2022.117764

Grotzinger, J., Bell, J., Herkenhoff, K., Johnson, J., Knoll, A., McCartney, E., et al. (2006). Sedimentary textures formed by aqueous processes, Erebus crater, Meridiani Planum, Mars. *Geology*, *34*(12), 1085–1088. https://doi.org/10.1130/g22985a.1

Haberle, R. M., McKay, C. P., Schaeffer, J., Cabrol, N. A., Grin, E. A., Zent, A. P., & Quinn, R. (2001). On the possibility of liquid water on present-day Mars. *Journal of Geophysical Research*, *106*(E10), 23317–23326. https://doi.org/10.1029/2000je001360

Haltigin, T. W., Pollard, W. H., Dutilleul, P., Osinski, G. R., & Koponen, L. (2014). Co-evolution of polygonal and scalloped terrains, southwestern Utopia Planitia, Mars. *Earth and Planetary Science Letters*, *387*, 44–54. https://doi.org/10.1016/j.epsl.2013.11.005

Herkenhoff, K. E., Squyres, S. W., Arvidson, R., Bass, D. S., Bell, J. F., Bertelsen, P., et al. (2004). Evidence from opportunity's microscopic imager for water on Meridiani Planum. *Science*, *306*(5702), 1727–1730. https://doi.org/10.1126/science.1105286

Hersen, P. (2004). On the crescentic shape of barchan dunes. *European Physical Journal B: Condensed Matter and Complex Systems*, *37*(4), 507–514. https://doi.org/10.1140/epjb/e2004-00087-y

Kirk, R. L., Howington-Kraus, E., Rosiek, M. R., Anderson, J. A., Archinal, B. A., Becker, K. J., et al. (2008). Ultrahigh resolution topographic mapping of Mars with MRO HiRISE stereo images: Meter-scale slopes of candidate Phoenix landing sites. *Journal of Geophysical Research*, *113*(E3), E00A24. https://doi.org/10.1029/2007je003000

Kirk, R. L., Mayer, D. P., Fergason, R. L., Redding, B. L., Galuszka, D. M., Hare, T. M., & Gwinner, K. (2021). Evaluating stereo Digital Terrain Model quality at Mars rover landing sites with HRSC, CTX, and HiRISE images. *Remote Sensing*, *13*(17), 3511. https://doi.org/10.3390/rs13173511

Langevin, Y., Poulet, F., Bibring, J.-P., & Gondet, B. (2005). Sulfates in the north polar region of Mars detected by OMEGA/Mars Express. *Science*, *307*(5715), 1584–1586. https://doi.org/10.1126/science.1109091

Lapotre, M. G., Ewing, R. C., Lamb, M. P., Fischer, W. W., Grotzinger, J. P., Rubin, D. M., et al. (2016). Large wind ripples on Mars: A record of atmospheric evolution. *Science*, *353*(6294), 55–58. https://doi.org/10.1126/science.aaf3206

Levy, J., Head, J., & Marchant, D. (2009). Thermal contraction crack polygons on Mars: Classification, distribution, and climate implications from HiRISE observations. *Journal of Geophysical Research*, *114*(E1), E01007. https://doi.org/10.1029/2008je003273

Li, C., Zheng, Y., Wang, X., Zhang, J., Wang, Y., Chen, L., et al. (2022). Layered subsurface in Utopia Basin of Mars revealed by Zhurong rover radar. *Nature*, *610*(7931), 308–312. https://doi.org/10.1038/s41586-022-05147-5

Li, X., Yao, W., & Wang, H. (2023). Martian subsurface water ice prediction at the Tianwen-1 mission landing site. *Icarus*, *389*, 115268. https://doi.org/10.1016/j.icarus.2022.115268

Liang, X., Chen, W., Cao, Z., Wu, F., Lyu, W., Song, Y., et al. (2021). The navigation and terrain cameras on the Tianwen-1 Mars rover. *Space Science Reviews*, *217*(3), 37. https://doi.org/10.1007/s11214-021-00813-y

Liu, J. J., Li, C. L., Zhang, R. Q., Rao, W., Cui, X. F., Geng, Y., et al. (2022). Geomorphic contexts and science focus of the Zhurong landing site on Mars. *Nature Astronomy*, *6*(1), 65–71. https://doi.org/10.1038/s41550-021-01519-5

Liu, Y., Wu, X., Zhao, Y. S., Pan, L., Wang, C., Liu, J., et al. (2022). Zhurong reveals recent aqueous activities in Utopia Planitia, Mars. *Science Advances*, *8*(19), eabn8555. https://doi.org/10.1126/sciadv.abn8555

Lu, Y., Edgett, K. S., Wu, B., Wang, Y., Li, Z., Michael, G. G., et al. (2022). Aeolian disruption and reworking of TARs at the Zhurong rover field site, southern Utopia Planitia, Mars. *Earth and Planetary Science Letters*, *595*, 117785. https://doi.org/10.1016/j.epsl.2022.117785

Lu, Y., Edgett, K. S., & Wu, Y. Z. (2021). Ripples, transverse aeolian ridges, and dark-toned sand dunes on Mars: A case study in Terra Sabaea. *Journal of Geophysical Research: Planets*, *126*(10), e2021JE006953. https://doi.org/10.1029/2021je006953

McEwen, A. S., Eliason, E. M., Bergstrom, J. W., Bridges, N. T., Hansen, C. J., Delamere, W. A., et al. (2007). Mars Reconnaissance orbiter's high resolution imaging science experiment (HiRISE). *Journal of Geophysical Research*, *112*(E5), E05S02. https://doi.org/10.1029/2005je002605

McEwen, A. S., Ojha, L., Dundas, C. M., Mattson, S. S., Byrne, S., Wray, J. J., et al. (2011). Seasonal flows on warm Martian slopes. *Science*, *333*(6043), 740–743. https://doi.org/10.1126/science.1204816

McLennan, S. M., Bell, J. F., Calvin, W. M., Christensen, P. R., Clark, B. C., de Souza, P. A., et al. (2005). Provenance and diagenesis of the evaporite-bearing burns formation, Meridiani Planum, Mars. *Earth and Planetary Science Letters*, *240*(1), 95–121. https://doi.org/10.1016/j.epsl.2005.09.041

Mellon, M. T., & Sizemore, H. G. (2022). The history of ground ice at Jezero Crater Mars and other past, present, and future landing sites. *Icarus*, *371*, 114667. https://doi.org/10.1016/j.icarus.2021.114667

Möhlmann, D., & Thomsen, K. (2011). Properties of cryobrines on Mars. *Icarus*, *212*(1), 123–130. https://doi.org/10.1016/j.icarus.2010.11.025

Mutch, T. A., Arvidson, R. E., Binder, A. B., Huck, F. O., Levinthal, E. C., Liebes, S., Jr., et al. (1976). Fine particles on Mars: Observations with the Viking 1 lander cameras. *Science*, *194*(4260), 87–91. https://doi.org/10.1126/science.194.4260.87

Ojha, L., Wilhelm, M. B., Murchie, S. L., McEwen, A. S., Wray, J. J., Hanley, J., et al. (2015). Spectral evidence for hydrated salts in recurring slope lineae on Mars. *Nature Geoscience*, *8*(8), 829–832. https://doi.org/10.1038/ngeo2546

Palumbo, A. M., Head, J. W., & Wilson, L. (2020). Rainfall on Noachian Mars: Nature, timing, and influence on geologic processes and climate history. *Icarus*, *347*, 113782. https://doi.org/10.1016/j.icarus.2020.113782

Reiss, D. (2004). Absolute dune ages and implications for the time of formation of gullies in Nirgal Vallis, Mars. *Journal of Geophysical Research*, *109*(E6), E06007. https://doi.org/10.1029/2004je002251

Ryan, A. J., & Christensen, P. R. (2012). Coils and polygonal crust in the Athabasca Valles region, Mars, as evidence for a volcanic history. *Science*, *336*(6080), 449–452. https://doi.org/10.1126/science.1219437

Savitzky, A., & Golay, M. J. (1964). Smoothing and differentiation of data by simplified least squares procedures. *Analytical Chemistry*, *36*(8), 1627–1639. https://doi.org/10.1021/ac60214a047

Schatz, V., Tsoar, H., Edgett, K. S., Parteli, E. J. R., & Herrmann, H. J. (2006). Evidence for indurated sand dunes in the Martian north polar region. *Journal of Geophysical Research*, *111*(E4), E04006. https://doi.org/10.1029/2005je002514

Silvestro, S., Chojnacki, M., Vaz, D. A., Cardinale, M., Yizhaq, H., & Esposito, F. (2020). Megaripple migration on Mars. *Journal of Geophysical Research: Planets*, *125*(8), e2020JE006446. https://doi.org/10.1029/2020je006446

Soare, R. J., Conway, S. J., & Dohm, J. M. (2014). Possible ice-wedge polygons and recent landscape modification by "wet" periglacial processes in and around the Argyre impact basin, Mars. *Icarus*, *233*, 214–228. https://doi.org/10.1016/j.icarus.2014.01.034

Soare, R. J., Conway, S. J., Williams, J. P., Philippe, M., Mc Keown, L. E., Godin, E., & Hawkswell, J. (2021). Possible ice-wedge polygonisation in Utopia Planitia, Mars and its latitudinal gradient of distribution. *Icarus*, *358*, 114208. https://doi.org/10.1016/j.icarus.2020.114208

Viviano-Beck, C. E., Seelos, F. P., Murchie, S. L., Kahn, E. G., Seelos, K. D., Taylor, H. W., et al. (2014). Revised CRISM spectral parameters and summary products based on the currently detected mineral diversity on Mars. *Journal of Geophysical Research: Planets*, *119*(6), 1403–1431. https://doi.org/10.1002/2014je004627

Wilson, S. A., & Zimbelman, J. R. (2004). Latitude-dependent nature and physical characteristics of transverse aeolian ridges on Mars. *Journal of Geophysical Research*, *109*(E10), E10003. https://doi.org/10.1029/2004je002247

Wu, X., Mustard, J. F., Tarnas, J. D., Zhang, X., Das, E., & Liu, Y. (2021). Imaging Mars analog minerals' reflectance spectra and testing mineral detection algorithms. *Icarus*, *369*, 114644. https://doi.org/10.1016/j.icarus.2021.114644

Xu, W., Liu, X., Yan, Z., Li, L., Zhang, Z., Kuang, Y., et al. (2021). The MarSCoDe instrument suite on the Mars Rover of China's Tianwen-1 mission. *Space Science Reviews*, *217*(5), 1–58. https://doi.org/10.1007/s11214-021-00836-5

Ye, B., Huang, J., Michalski, J., & Xiao, L. (2019). Geomorphologic characteristics of polygonal features on chloride-bearing deposits on Mars: Implications for Martian hydrology and astrobiology. *Journal of Earth Sciences*, *30*(5), 1049–1058. https://doi.org/10.1007/s12583-019-1212-2

Zhao, J., Xiao, Z., Huang, J., Head, J. W., Wang, J., Shi, Y., et al. (2021). Geological characteristics and targets of high scientific interest in the Zhurong landing region on Mars. *Geophysical Research Letters*, *48*(20), e2021GL094903. https://doi.org/10.1029/2021gl094903

Zimbelman, J. R. (2010). Transverse aeolian ridges on Mars: First results from HiRISE images. *Geomorphology*, *121*(1–2), 22–29. https://doi.org/10.1016/j.geomorph.2009.05.012

Zimbelman, J. R., & Foroutan, M. (2020). Dingo Gap: Curiosity went up a small transverse aeolian ridge and came down a megaripple. *Journal of Geophysical Research: Planets*, *125*(12), e2020JE006489. https://doi.org/10.1029/2020je006489

Zimbelman, J. R., Williams, S. H., & Johnston, A. K. (2012). Cross-sectional profiles of sand ripples, megaripples, and dunes: A method for discriminating between formational mechanisms. *Earth Surface Processes and Landforms*, *37*(10), 1120–1125. https://doi.org/10.1002/esp.3243